Supporting Information

3D printing of cellulose nanocrystals-loaded hydrogels through rapid fixation by photopolymerization

Doron Kam[12], Ariel Braner[13], Avi Abouzglo[1], Liraz Larush[1], Annalisa Chiappone[4], Oded Shoseyov[2], Shlomo Magdassi[1]**

[1]Institute of Chemistry, The Hebrew University of Jerusalem, Jerusalem, Israel

[2]Plant Sciences and Genetics in Agriculture, The Hebrew University of Jerusalem, Rehovot, Israel

[3]Alpha program, Future scientist center, Jerusalem, Israel

[4]Department of Applied Science and Technology, Politecnico di Torino, Torino, Italy.

Corresponding Authors

*Oded Shoseyov: shoseyov@agri.huji.ac.il

*Shlomo Magdassi: magdassi@mail.huji.ac.il

Table of contents:

Figure S1. Summary of photocurable hydrogels	**S3**
Table S1. Summary of photocurable hydrogels based on one-time illumination	**S4**
Table S2. Summary of photocurable hydrogels based on build time	**S5**
Supporting information section S1: Estimating printing maximum shear rate (MSR)	**S6**
Figure S3. Raw data of unconfined compression test	**S8**
Figure S4. Oscillation amplitude sweep	**S9**
Figure S5. Oscillation frequency sweep	**S10**
Supporting information section S2: Polymerization kinetics of acrylic acid by FTIR	**S11**
Figure S9. Printed tube without rapid photopolymerization	**S14**
Figure S10. Printed tube with rapid photopolymerization	**S15**
Figure S11. Extrusion width compared to nozzle width	**S16**
Figure S12. Printability value	**S16**
Figure S13. Correlation between the designed area to the calculated area	**S17**
Figure S14. High aspect ratio photo	**S17**
Figure S15. Maximum reached overhang	**S18**
Figure S16. Comparison between different wavelength irradiation	**S19**
References	**S20**

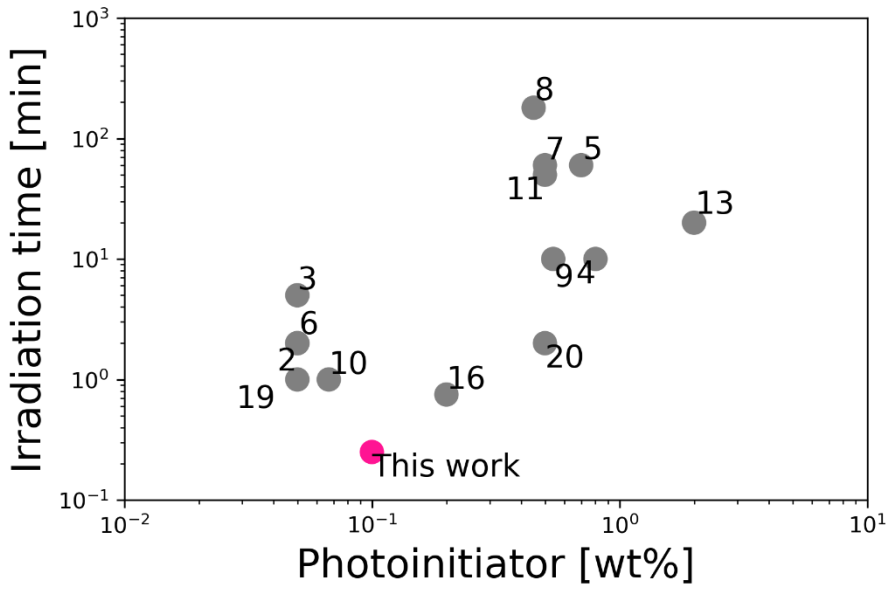

(A)

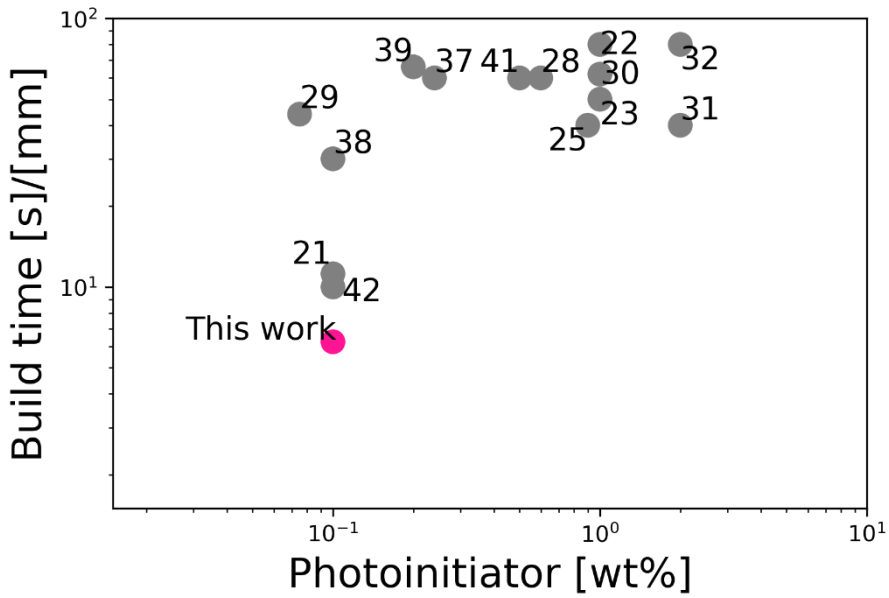

(B)

Figure S1. Summary of photocurable hydrogels. PI concentration based on (A) One-time illumination (mold or post-curing) (B) build time (various 3D printing techniques). See Table S1-2.

Table S1. Summary of photocurable hydrogels based on one-time illumination. The best numbers (smallest PI concentration and the fastest irradiation time) were taken from the manuscript. ? indicate unknown parameter, ∞ indicate continues irradiation.

Materials	Process	Liquid phase	Photoinitiator (PI)	PI [wt %]	Light source [nm]	Irradiation time [min]	Ref.
CNC, AAc, PEGDA	DIW	water	Water soluble TPO	0.1	395	0.25	This work
GA, isoleucine, nitrobenzyl	DIW	water	photocleavage of nitrobenzyl	?	365	20	[1]
HA	DIW	PBS	Irgacure 2959	0.05	365	2	[2]
HA	DIW	Water/PBS	Irgacure 2959	0.05	320-390	5	[3]
GelMA	DIW	water	Li-TPO-L	0.8	365	10	[4]
AAm, BisAAm	DIW	water	Irgacure 2959	0.7	375	60	[5]
HA	DIW	water	Irgacure 2959	0.05	312	2	[6]
CNC, AAm, BisAAm	mold	water	2,2-diethoxyacetophenone	0.5	300	60	[7]
CNC, AAm, BisAAm	mold	water	Irgacure 2959	0.45	300	180	[8]
CNC, phenyl acrylate, AAm	DIW	DMSO	Irgacure 2959	0.54	365	10	[9]
CNC, PEGDA	DIW	water	LAP	0.067	365	1	[10]
CNC, PDMA	mold	water	2,2-diethoxyacetophenone	0.5	365	50	[11]
CNC-BAPO, MMA, BuA, NIPAAm, HEA	mold	DMF	BAPO	?	?	60	[12]
cin-CNC, PUA	DIW	isopropanol	Irgacure 819	2	410	20	[13]
CNC, AAc, DES	DIW	Ethylene glycol	Irgacure 2959	?	365	30	[14]
GelMA, PEGDMA, Chitosan	DIW	water	Irgacure 2959	0.5	?	?	[15]
GelMA	DIW	PBS	LAP	0.2	365	0.75	[16]
Poly(alkyl glycidyl ether)	DIW	water	2-hydroxy-2-methylpropiophenone	?	365	3	[17]
GelMA, HA	DIW	water	LAP	0.5	Blue light	∞	[18]
hASCs, hMSCs	DIW	water	Irgacure 2959	0.05	UV	1	[19]
Gelatin	mold	PBS	Irgacure 2959	0.5	365	2	[20]

Acrylic acid (AAc), Acrylamide (AAm), N,N'-methylenebisacrylamide (BisAAm), poly(N,N-dimethylacrylamide) (PDMA), methyl methacrylate (MMA), butyl acrylate (BuA), N-isopropylacrylamide (NIPAAm), Deep eutectic solvent (DES), 2-hydroxyethyl acrylate (HEA), Polypeptide glutamic acid (GA), polyether urethane acrylate (PUA), Hyaluronic acid (HA), Cinnamoyl chloride (cin), Poly(ethylene glycol) diacrylate (PEGDA), Direct ink writing (DIW), diphenyl(2,4,6-trimethylbenzoyl)phosphine oxide (TPO) 2-Hydroxy-4′-(2-hydroxyethoxy)-2-methylpropiophenone (Irgacure 2959), lithium phenyl-2,4,6-trimethylbenzoylphosphinate (LAP), Phenylbis(2,4,6-trimethyl- benzoyl) phosphine oxide (Irgacure 819), bis(acyl)phosphane oxide (BAPO), Human adipose-derived stem cells (hASCs) human bone marrow-derived mesenchymal stem cells (hMSCs)

Table S2. Summary of photocurable hydrogels based on build time. The best numbers (smallest PI concentration and the fastest build time) were taken from the manuscript. ? indicate unknown parameter, ∞ indicate continues irradiation.

Materials	Process	Liquid phase	Photoinitiator	PI [wt%]	Light source [nm]	layer exposure time [s]	Layer thickness [mm]	Build time [s]/[mm]	Post curing time [min]	Ref.
CNC, AAc, PEGDA	DIW	water	Water soluble TPO	0.1	365/405	5	0.8	6.25	0	This work
GelMA	DIW	PBS	Irgacure 2959	0.1	365	2.8	0.25	11.2	0	[21]
GelMA	DMD	PBS	Irgacure 2959	1	UV	8	0.1	80	0	[22]
PEGDA	DMD		LAP	1	UV	1.25	0.025	50	0	[23]
M-CMC	DLP	water	LAP	0.4	385	?	0.05		?	[24]
CNC, PEGDA, DiGlyDA,	DLP	-	Irgacure 819	0.9	?	4	0.1	40	0	[25]
CNC-BAPO, PEGMEM,	DLP	water	BAPO	?	405	3	0.02	150	5	[26]
PEGDMA	SLA	PEGDMA	Irgacure 2959/TPO	1	405	?	0.05		10	[27]
Silk fibroin	DLP	PBS	LAP	0.6	365	3	0.05	60	0	[28]
MA-BSA	SLA	water	Ru(bpy)3Cl	0.075	405	2.2	0.05	44	90	[29]
PEGDA	DMD	PBS	LAP	1	405	3.1	0.05	62	0	[30]
TMAEA, NVP	DLP	water	TPO	2	405	2	0.05	40	10	[31]
PEGDA	DLP	water	TPO	2	365	2	0.025	80	0	[32]
CNC, PEGDA	SLA	water	LAP	0.75	405	?	0.05		0	[33]
CNC, HEMA, PUA	DIW	Isopropanol / ethanol (3:1)	Irgacure 819	0.5	UV	a few minutes	?		0	[34]
HA	DIW	water	Irgacure 2959	0.05	UV	∞	?		5	[35]
AA	DMD	AA	Irgacure 2959	10	365	10	?		0	[36]
AAm	SLA	water	TPO	0.24	385	6	0.1	60	0	[37]
AA	DLP	water	TPO	0.1	385	3	0.1	30	0	[38]
Chitosan	DLP	water	LAP	0.2	?	10	0.15	66	0	[39]
Acr-PGS	DIW	Acr-PGS	DMPA	0.5	UV	∞	?		5	[40]
PEDOT:PSS, PEGDA	mold	water	BAPO	0.5	UV	60	1	60	0	[41]
PEGDA, Poloxamer	DIW	Water	Irgacure 2959	0.1	UV	2	0.2	10	60	[42]

Acrylic acid (AAc), Acrylamide (AAm), 2-hydroxyethyl methacrylate (HEMA), polyether urethane acrylate (PUA), Hyaluronic acid (HA), Poly(ethylene glycol) diacrylate (PEGDA), glycerol 1,3-diglycerolate diacrylate (DiGlyDA), Direct ink writing (DIW), digital light projector (DLP), digital micromirror device (DMD), Stereolithography (SLA), diphenyl(2,4,6-trimethylbenzoyl)phosphine oxide (TPO) 2-Hydroxy-4′-(2-hydroxyethoxy)-2-methylpropiophenone (Irgacure 2959), lithium phenyl-2,4,6-trimethylbenzoylphosphinate (LAP), Phenylbis(2,4,6-trimethyl- benzoyl) phosphine oxide (Irgacure 819), bis(acyl)phosphane oxide (BAPO), acrylated polyglycerol sebacate (Acr-PGS), 2,2-dimethoxy-2-phenylacetophenone (DMPA), Trimethylammonium ethyl acrylate chloride (TMAEA), N-vinyl pyrrolidone (NVP), Methacrylated bovine serum albumin (MA-BSA), Methacrylated-CMC (M-CMC)

Supporting information section S1: Estimating printing maximum shear rate (MSR)

The shear rate in a pipe for Newtonian behavior is defined as:

$$\dot{\gamma_N} = \frac{4Q}{\pi R^3} \quad Eq.S1$$

Where R is defined as the radius of the pipe, and Q is the volumetric flow rate. For shear-thinning fluids (pseudoplastic) Rabinowitsch correction is necessary. For the power-law model ($\eta = k\dot{\gamma}^{n-1}$) the shear rate becomes:

$$\dot{\gamma_P} = \frac{3n+1}{4n}\frac{4Q}{\pi R^3} \quad Eq.S2$$

The volumetric flow rate is defined as volume per unit time and can also be defined as flow viscosity times cross-sectional area. Through our 3D printer, it is hard to determine the flow viscosity inside the syringe nozzle, therefore we can estimate Q from the printed material:

$$Q = \pi R^2 \vec{s} = DH\vec{v} \quad Eq.S3$$

Where the flow speed inside the syringe is $\vec{s}$, $\vec{v}$ is the printing speed, R is defined as the nozzle radius, D as the path width ($D = 2R$), and H is the path height (layer thickness). For $D = 0.64\ mm, H = 0.3\ mm\ and\ \vec{v} = 10\frac{mm}{s}$, we calculate $Q = 1.92\frac{mm^3}{s}$.

The flow rate can be measured by a constant rate plate rheology. First, a constant low shear rate ($\dot{\gamma}$=0.01 1/s, t=100s, T=20 °C) was applied to allow the sample to reach the set temperature (20°) and to achieve a defined shear history before the actual

experiment. Then, shear rate ramp-up ($\dot{\gamma}$=0.01 1/s to $\dot{\gamma}$=100 1/s, t=100 s, T=20 °C). Each sample was measured three times (Figure S2).

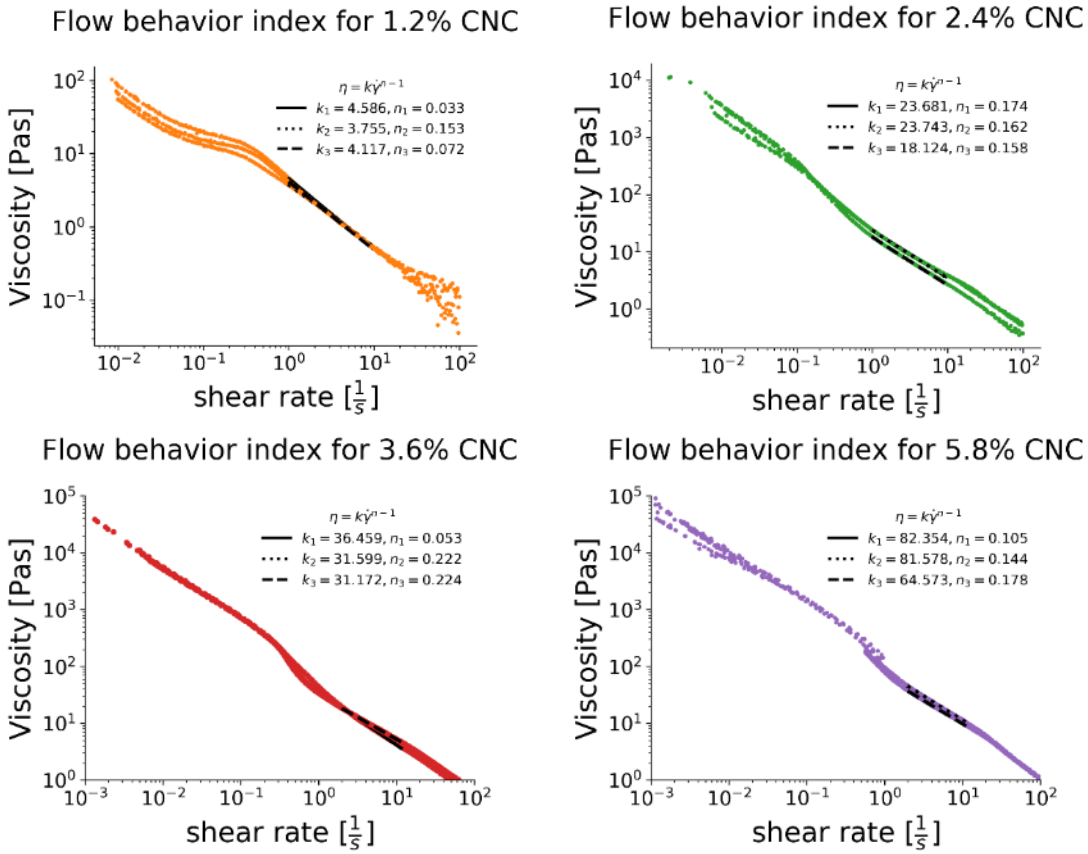

Figure S2. Raw data of viscosity over shear rate to determine flow behavior index by fitting $\eta = k\dot{\gamma}^{n-1}$ between $1 < \dot{\gamma} < 10$.

A power-law model ($\eta = k\dot{\gamma}^{n-1}$) was used to fit a function between $1\frac{1}{s} < \dot{\gamma} < 10\frac{1}{s}$, using a non-linear least-squares method. Based on Eq. S1-2 maximum shear rate was calculated (Table S3).

Table S3. Calculated maximum shear rate (MSR)

	1.2% CNC	2.4% CNC	3.6% CNC	5.8% CNC
n	0.09	0.165	0.17	0.14
MSR (power law) [1/s]	273	169	168	187
MSR (Newtonian) [1/s]		75		

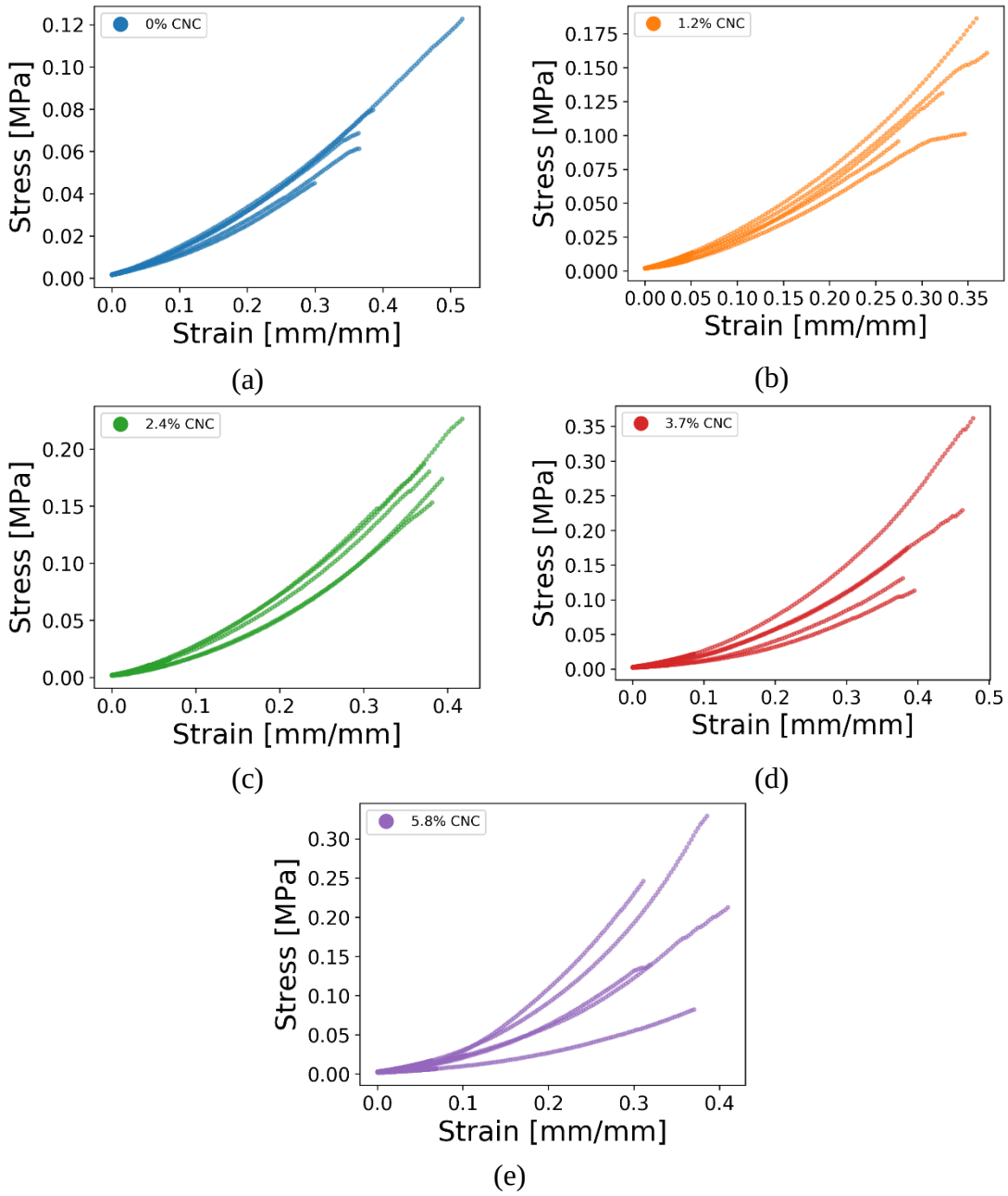

Figure S3. Raw data of five replicates of unconfined compression test of hydrogels with different amount of CNC wt% (a) 0% CNC (b) 1.2% CNC (c) 2.4% CNC (d) 3.7% CNC (e) 5.8% CNC.

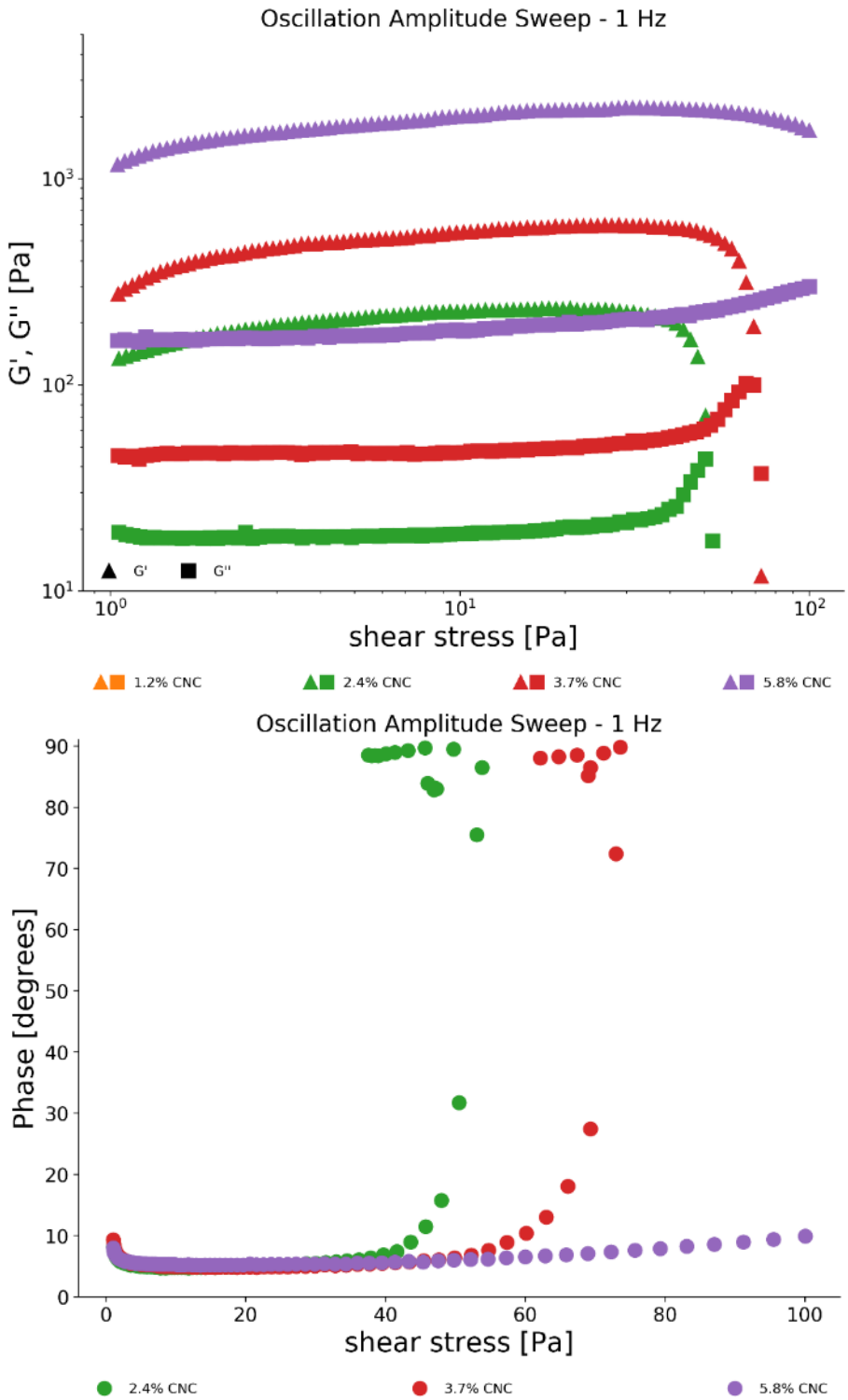

Figure S4. (**Top**) Oscillation amplitude sweep at 1Hz. Shear storage (G') and shear loss moduli (G'') (**Bottom**) Oscillation amplitude sweep at 1Hz, phase plot. Low phase angles indicate "solid-like" behaviour while high phase angles indicate "liquid-like" behaviour.

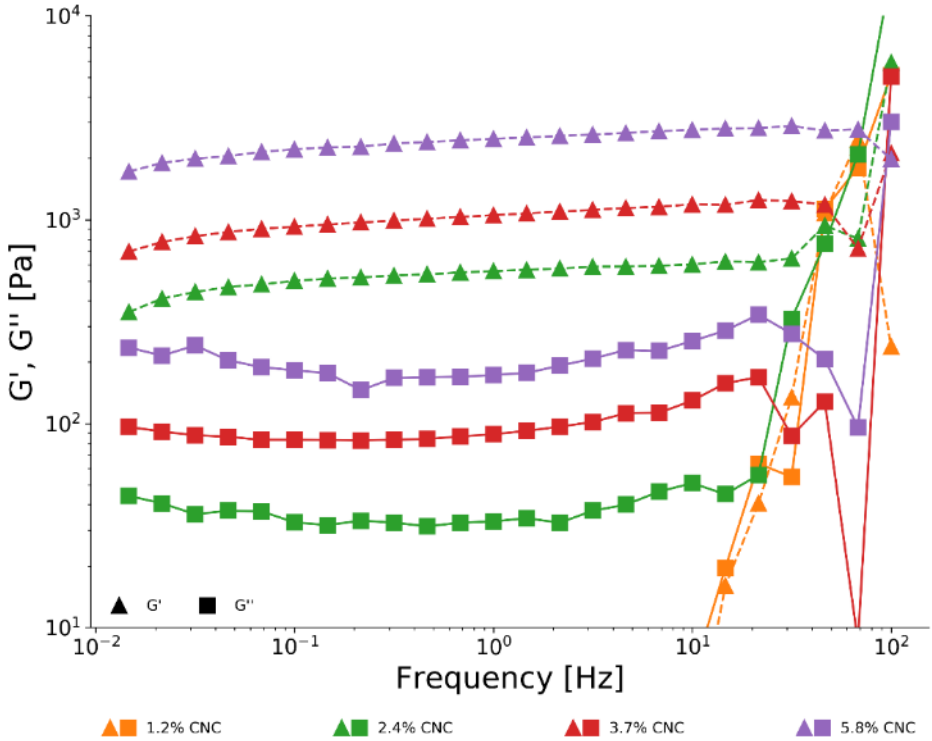

Figure S5. Oscillation frequency sweep at 10 Pa. Shear storage (G') and shear loss moduli (G'') as a function of frequency for different samples.

Supporting information section S2: Polymerization kinetics of acrylic acid by FTIR

Infrared absorption measurements were performed to evaluate polymerization kinetics of ink 2.4% CNC using IRAffinity-1S Fourier Transform Infrared Spectrophotometer (Shimadzu Corp., Kyoto, Japan) equipped with diamond ATR attachment and activated by LabSolutions IR software (Shimadzu Corp., Kyoto, Japan). Unpolymerized ink and fully photo-polymerized ink by irradiation of LED light (365nm or 405nm 50W LED, Shenzhen Justar Electronic Technology CO. LTD, China) for 20 s, spectra were acquired by 20 scans of FTIR collected over the spectral range of $1800 - 800\ cm^{-1}$ with instrument resolution of $2\ cm^{-1}$.

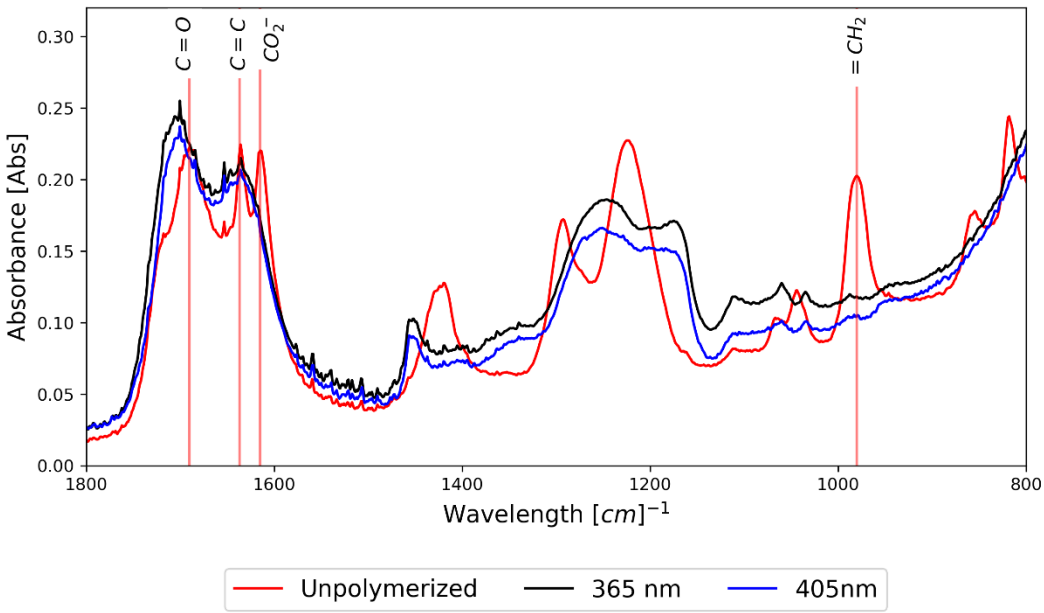

Figure S6. FTIR spectra of ink 2.4% CNC before and after light irradiation.

Figure S6 shows that Acrylic Acid (AA) monomer (unpolymerized) possessed absorption peaks due to signals at $1639\ cm^{-1}$ that is associated to the $C = C$ bond and $984\ cm^{-1}$ signal that is associated to the $= CH_2$ bond. These peaks disappeared after photopolymerization, revealing the reaction of the carbon-carbon double bond.[43] Moreover, $C = O$ stretch at $1690\ cm^{-1}$ is enhanced while the asymmetric stretch of CO_2^- at $1615\ cm^{-1}$ decreases, pertaining transformation of proton.[44]

Based on these finding, FTIR kinetic monitoring of the polymerization of AA in 2.4% CNC sample were performed on ~200 µl of ink dropped on the ATR diamond during light irradiation, followed by acquiring continuous spectra (1 scan per 3s, with instrument resolution of 8 cm^{-1}) within the two ranges $1800 - 1500\ cm^{-1}$ and $1100 - 900\ cm^{-1}$ (Figure S7).

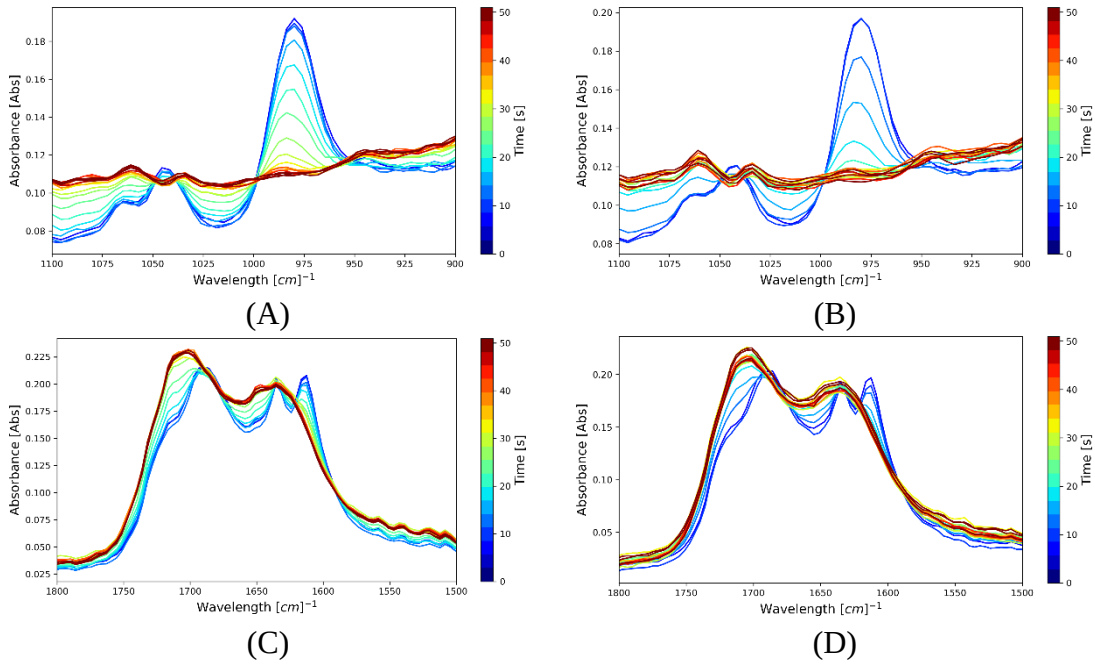

Figure S7. Polymerization kinetics. Fourier transform infrared spectrum of $C = C$ acquired after every 3 seconds using (A, C) 365nm and (B, D) 405 nm LED light.

The polymerization conversion rate (CR) of AA was calculated from the decay/disappearance of the absorption peaks of the carbon-carbon double bonds according to the Beer–Lambert law, normalized to the final absorbance peak:

$$CR = \frac{1 - \frac{A_t}{A_0}}{1 - \frac{A_\infty}{A_0}} \cdot 100 \quad Eq.S4$$

Where A_0, A_∞ *and* A_t are the absorbances of the peak at time 0, fully polymerized, and at time t.[37,45]

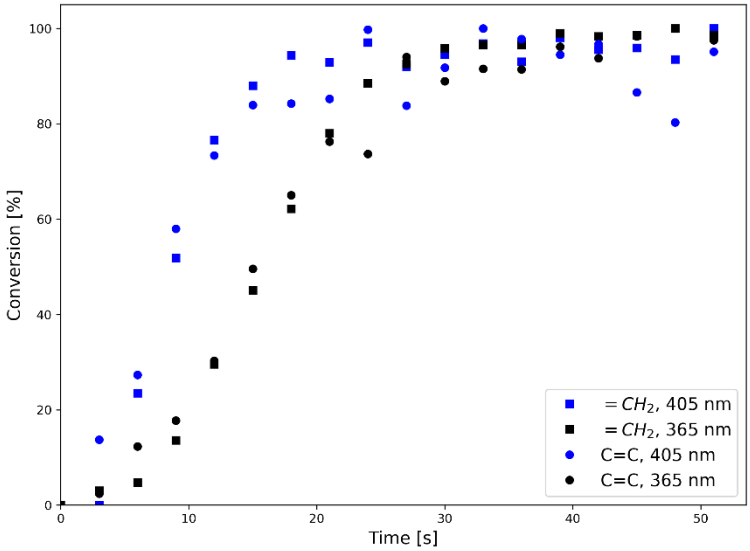

Figure S8. Percentage of conversion of carbon-carbon double bond using Eq. S4.

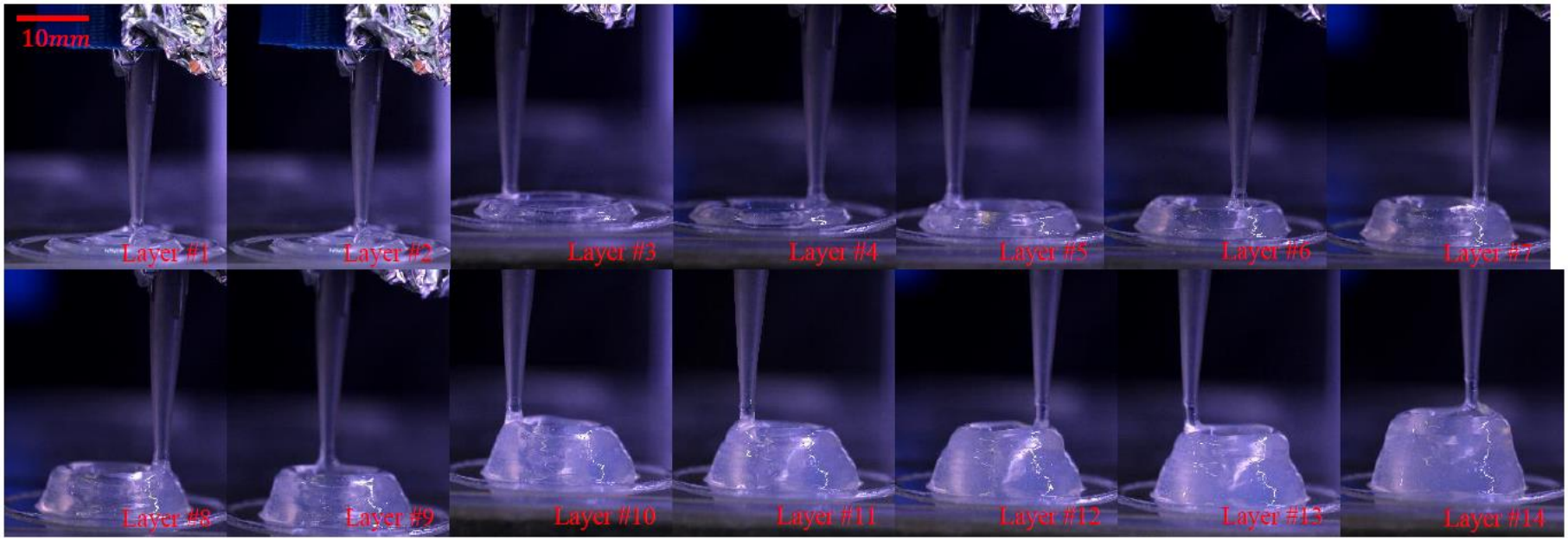

Figure S9. Tube printed by DIW method with 2.4% CNC ink without rapid UV photographed after each layer.

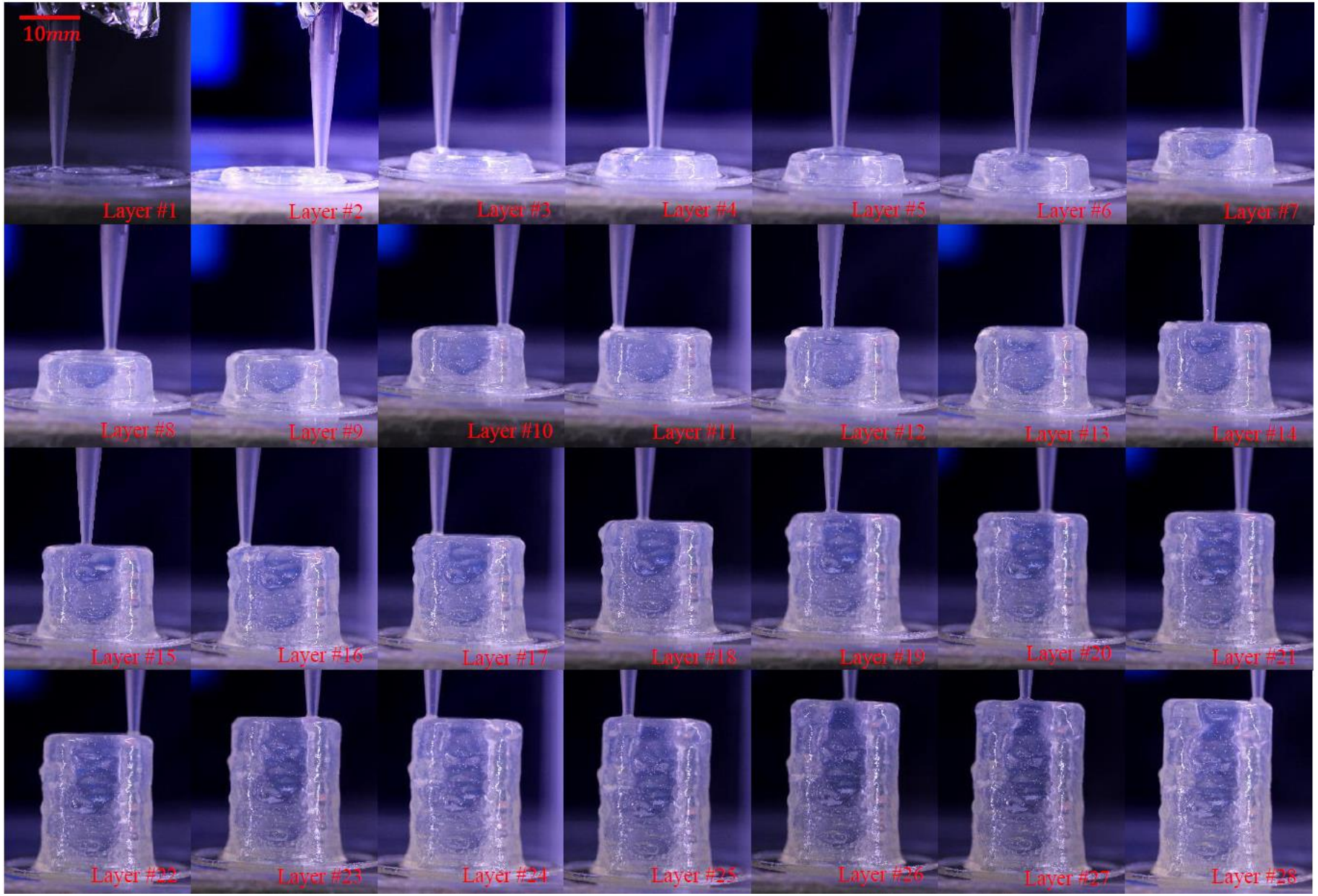

Figure S10. Tube printed by DIW method with 2.4% CNC ink with rapid UV photographed after each layer.

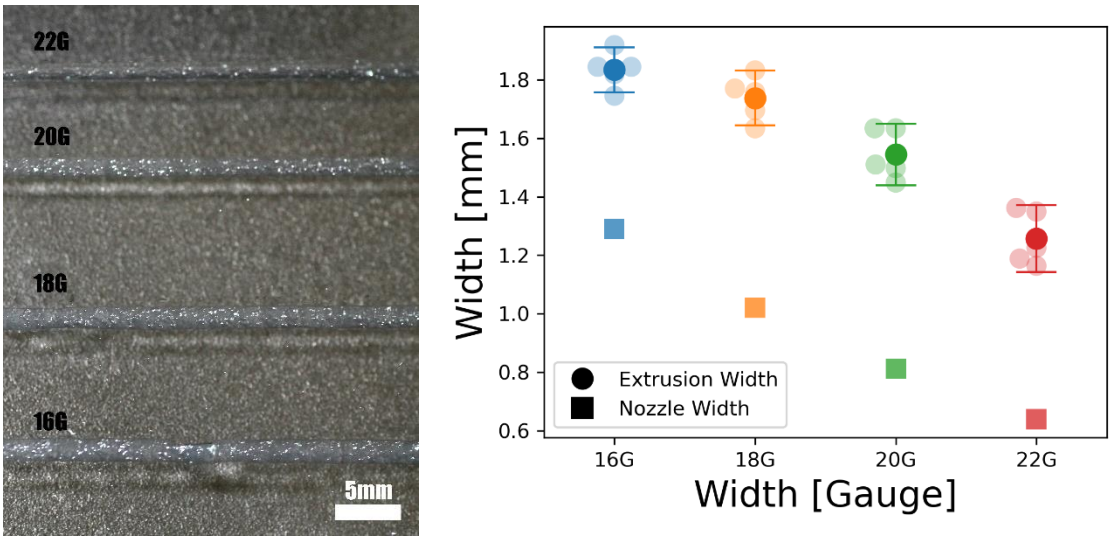

(A) (B)

Figure S11. Printing ink containing 2.4% CNC using different nozzle diameters; 16G (1.29 mm), 18G (1.02 mm), 20G (0.81 mm), 22G (0.64 mm) (A) photo of printed lines (B) width of the printed line and nozzle diameter for the various nozzles.

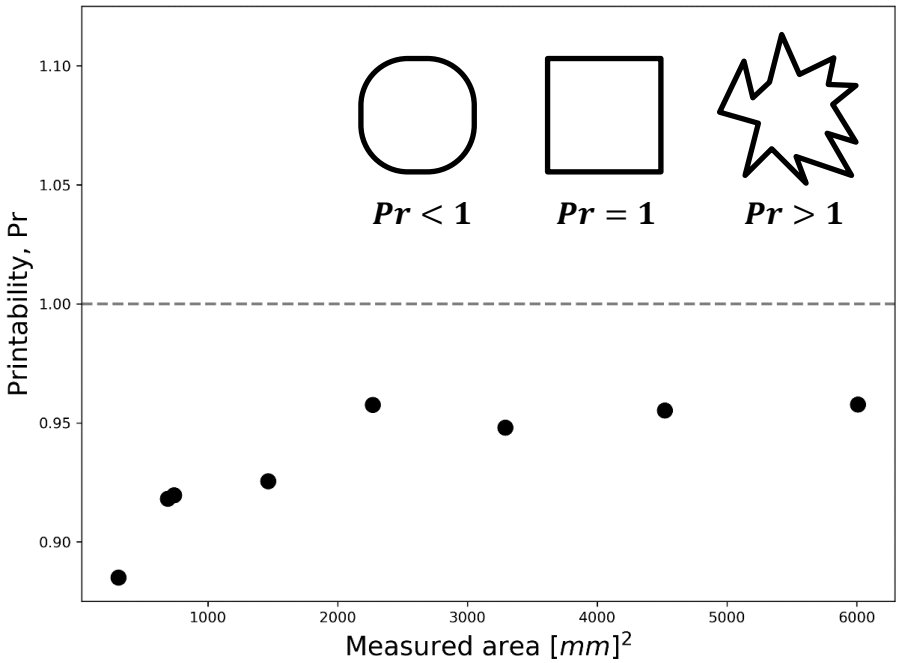

Figure S12. Printability value of printed square objects at different area sizes.

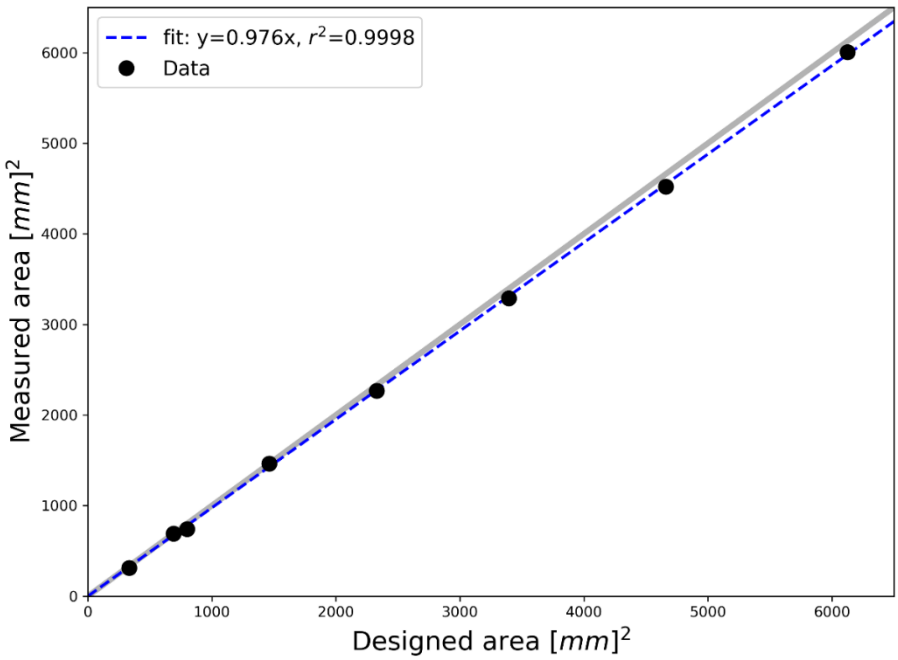

Figure S13. Correlation between the designed area to the calculated area measured by photographed squares.

Figure S14. High aspect ratio (~13) printed hydrogel object using 2.4% CNC ink.

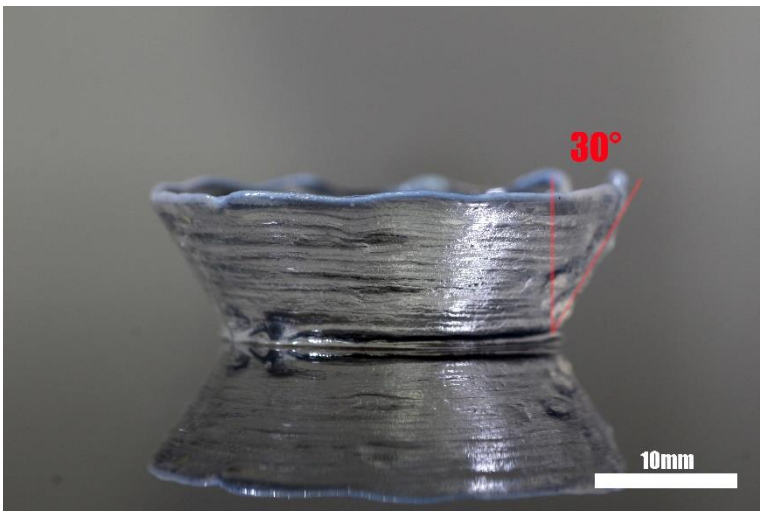

Figure S15. Maximum reached overhang for 2.4% CNC using 1.29 mm nozzle.

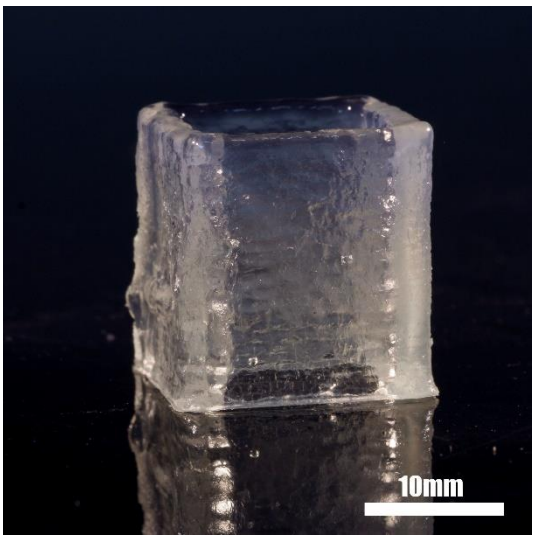

(A)

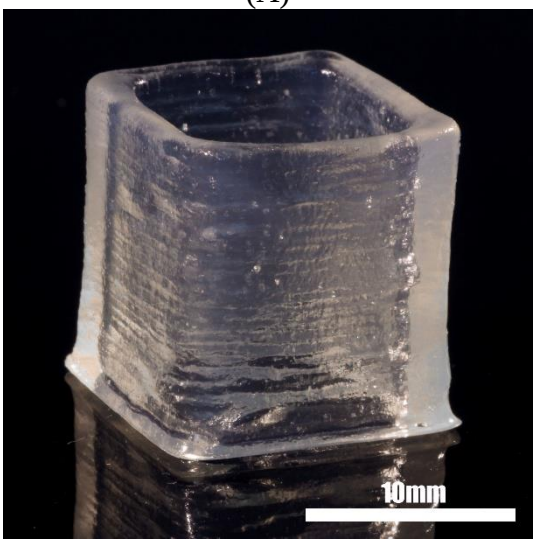

(B)

Figure S16. Printing cube from ink containing 2.4% CNC by different wavelength irradiation (A) 365 nm (B) 405 nm.

References

(1) Murphy, R. D.; Kimmins, S.; Hibbitts, A. J.; Heise, A. 3D-Extrusion Printing of Stable Constructs Composed of Photoresponsive Polypeptide Hydrogels. *Polym. Chem.* **2019**, *10* (34), 4675–4682. https://doi.org/10.1039/c9py00796b.

(2) Wang, L. L.; Highley, C. B.; Yeh, Y. C.; Galarraga, J. H.; Uman, S.; Burdick, J. A. Three-Dimensional Extrusion Bioprinting of Single- and Double-Network Hydrogels Containing Dynamic Covalent Crosslinks. *J. Biomed. Mater. Res. - Part A* **2018**, *106* (4), 865–875. https://doi.org/10.1002/jbm.a.36323.

(3) Highley, C. B.; Rodell, C. B.; Burdick, J. A. Direct 3D Printing of Shear-Thinning Hydrogels into Self-Healing Hydrogels. *Adv. Mater.* **2015**, *27* (34), 5075–5079. https://doi.org/10.1002/adma.201501234.

(4) Tytgat, L.; Van Damme, L.; Ortega Arevalo, M. del P.; Declercq, H.; Thienpont, H.; Otteveare, H.; Blondeel, P.; Dubruel, P.; Van Vlierberghe, S. Extrusion-Based 3D Printing of Photo-Crosslinkable Gelatin and κ-Carrageenan Hydrogel Blends for Adipose Tissue Regeneration. *Int. J. Biol. Macromol.* **2019**, *140*, 929–938. https://doi.org/10.1016/j.ijbiomac.2019.08.124.

(5) Wei, J.; Wang, J.; Su, S.; Wang, S.; Qiu, J.; Zhang, Z.; Christopher, G.; Ning, F.; Cong, W. 3D Printing of an Extremely Tough Hydrogel. *RSC Adv.* **2015**, *5* (99), 81324–81329. https://doi.org/10.1039/c5ra16362e.

(6) Kiyotake, E. A.; Douglas, A. W.; Thomas, E. E.; Nimmo, S. L.; Detamore, M. S. Development and Quantitative Characterization of the Precursor Rheology of Hyaluronic Acid Hydrogels for Bioprinting. *Acta Biomater.* **2019**, *95*, 176–187. https://doi.org/10.1016/j.actbio.2019.01.041.

(7) Kelly, J. A.; Shukaliak, A. M.; Cheung, C. C. Y.; Shopsowitz, K. E.; Hamad, W. Y.; MacLachlan, M. J. Responsive Photonic Hydrogels Based on Nanocrystalline Cellulose. *Angew. Chemie - Int. Ed.* **2013**, *52* (34), 8912–8916. https://doi.org/10.1002/anie.201302687.

(8) Wang, P.-X.; Hamad, W. Y.; MacLachlan, M. J. Structure and Transformation of Tactoids in Cellulose Nanocrystal Suspensions. *Nat. Commun.* **2016**, *7* (1), 11515. https://doi.org/10.1038/ncomms11515.

(9) Zhang, Z.; Liu, R.; Zepeda, H.; Zeng, L.; Qiu, J.; Wang, S. 3D Printing Super Strong Hydrogel for Artificial Meniscus. *ACS Appl. Polym. Mater.* **2019**, *1* (8), 2023–2032. https://doi.org/10.1021/acsapm.9b00304.

(10) Frost, B.; Sutliff, B. P.; Thayer, P.; Bortner, M. J.; Foster, E. J. Gradient Poly(Ethylene Glycol) Diacrylate and Cellulose Nanocrystals Tissue Engineering Composite Scaffolds via Extrusion Bioprinting. *Front. Bioeng. Biotechnol.* **2019**, *7* (OCT), 1–14. https://doi.org/10.3389/fbioe.2019.00280.

(11) Yang, J.; Han, C. R.; Xu, F.; Sun, R. C. Simple Approach to Reinforce Hydrogels with Cellulose Nanocrystals. *Nanoscale* **2014**, *6* (11), 5934–5943. https://doi.org/10.1039/c4nr01214c.

(12) Wang, J.; Siqueira, G.; Müller, G.; Rentsch, D.; Huch, A.; Tingaut, P.; Levalois-Grützmacher, J.; Grützmacher, H. Synthesis of New Bis(Acyl)Phosphane Oxide Photoinitiators for the Surface Functionalization of Cellulose Nanocrystals. *Chem. Commun.* **2016**, *52* (13), 2823–2826. https://doi.org/10.1039/c5cc09760f.

(13) Müller, L. A. E.; Zimmermann, T.; Nyström, G.; Burgert, I.; Siqueira, G. Mechanical Properties Tailoring of 3D Printed Photoresponsive Nanocellulose

Composites. *Adv. Funct. Mater.* **2020**, *2002914*, 2002914. https://doi.org/10.1002/adfm.202002914.

(14) Lai, C. W.; Yu, S. S. 3D Printable Strain Sensors from Deep Eutectic Solvents and Cellulose Nanocrystals. *ACS Appl. Mater. Interfaces* **2020**, *12* (30), 34235–34244. https://doi.org/10.1021/acsami.0c11152.

(15) Mora-Boza, A.; Włodarczyk-Biegun, M. K.; Del Campo, A.; Vázquez-Lasa, B.; Román, J. S. Glycerylphytate as an Ionic Crosslinker for 3D Printing of Multi-Layered Scaffolds with Improved Shape Fidelity and Biological Features. *Biomater. Sci.* **2020**, *8* (1), 506–516. https://doi.org/10.1039/c9bm01271k.

(16) Ding, H.; Illsley, N. P.; Chang, R. C. 3D Bioprinted GelMA Based Models for the Study of Trophoblast Cell Invasion. *Sci. Rep.* **2019**, *9* (1), 1–13. https://doi.org/10.1038/s41598-019-55052-7.

(17) Johnston, T. G.; Fellin, C. R.; Carignano, A.; Nelson, A. Poly(Alkyl Glycidyl Ether) Hydrogels for Harnessing the Bioactivity of Engineered Microbes. *Faraday Discuss.* **2019**, *219*, 58–72. https://doi.org/10.1039/c9fd00019d.

(18) Wang, Y.; Li, Y.; Yu, X.; Long, Q.; Zhang, T. Synthesis of a Photocurable Acrylated Poly(Ethylene Glycol)-: Co -Poly(Xylitol Sebacate) Copolymers Hydrogel 3D Printing Ink for Tissue Engineering. *RSC Adv.* **2019**, *9* (32), 18394–18405. https://doi.org/10.1039/c9ra03637g.

(19) Jeon, O.; Lee, Y. Bin; Jeong, H.; Lee, S. J.; Wells, D.; Alsberg, E. Individual Cell-Only Bioink and Photocurable Supporting Medium for 3D Printing and Generation of Engineered Tissues with Complex Geometries. *Mater. Horizons* **2019**, *6* (8), 1625–1631. https://doi.org/10.1039/c9mh00375d.

(20) Li, L.; Lu, C.; Wang, L.; Chen, M.; White, J.; Hao, X.; McLean, K. M.; Chen, H.; Hughes, T. C. Gelatin-Based Photocurable Hydrogels for Corneal Wound Repair. *ACS Appl. Mater. Interfaces* **2018**, *10* (16), 13283–13292. https://doi.org/10.1021/acsami.7b17054.

(21) Zhuang, P.; Ng, W. L.; An, J.; Chua, C. K.; Tan, L. P. Layer-by-Layer Ultraviolet Assisted Extrusion-Based (UAE) Bioprinting of Hydrogel Constructs with High Aspect Ratio for Soft Tissue Engineering Applications. *PLoS One* **2019**, *14* (6), 1–21. https://doi.org/10.1371/journal.pone.0216776.

(22) Grogan, S. P.; Chung, P. H.; Soman, P.; Chen, P.; Lotz, M. K.; Chen, S.; D'Lima, D. D. Digital Micromirror Device Projection Printing System for Meniscus Tissue Engineering. *Acta Biomater.* **2013**, *9* (7), 7218–7226. https://doi.org/10.1016/j.actbio.2013.03.020.

(23) Huang, T. Q.; Qu, X.; Liu, J.; Chen, S. 3D Printing of Biomimetic Microstructures for Cancer Cell Migration. *Biomed. Microdevices* **2014**, *16* (1), 127–132. https://doi.org/10.1007/s10544-013-9812-6.

(24) Melilli, G.; Carmagnola, I.; Tonda-Turo, C.; Pirri, F.; Ciardelli, G.; Sangermano, M.; Hakkarainen, M.; Chiappone, A. DLP 3D Printing Meets Lignocellulosic Biopolymers: Carboxymethyl Cellulose Inks for 3D Biocompatible Hydrogels. *Polymers (Basel).* **2020**, *12* (8), 1–11. https://doi.org/10.3390/POLYM12081655.

(25) Li, V. C. F.; Kuang, X.; Mulyadi, A.; Hamel, C. M.; Deng, Y.; Qi, H. J. 3D Printed Cellulose Nanocrystal Composites through Digital Light Processing. *Cellulose* **2019**, *26* (6), 3973–3985. https://doi.org/10.1007/s10570-019-02353-9.

(26) Wang, J.; Chiappone, A.; Roppolo, I.; Shao, F.; Fantino, E.; Lorusso, M.;

Rentsch, D.; Dietliker, K.; Pirri, C. F.; Grützmacher, H. All-in-One Cellulose Nanocrystals for 3D Printing of Nanocomposite Hydrogels. *Angew. Chemie - Int. Ed.* **2018**, *57* (9), 2353–2356. https://doi.org/10.1002/anie.201710951.

(27) Burke, G.; Devine, D. M.; Major, I. Effect of Stereolithography 3d Printing on the Properties of Pegdma Hydrogels. *Polymers (Basel).* **2020**, *12* (9), 1–13. https://doi.org/10.3390/polym12092015.

(28) Hong, H.; Seo, Y. B.; Kim, D. Y.; Lee, J. S.; Lee, Y. J.; Lee, H.; Ajiteru, O.; Sultan, M. T.; Lee, O. J.; Kim, S. H.; Park, C. H. Digital Light Processing 3D Printed Silk Fibroin Hydrogel for Cartilage Tissue Engineering. *Biomaterials* **2020**, *232* (November 2019), 119679. https://doi.org/10.1016/j.biomaterials.2019.119679.

(29) Smith, P. T.; Narupai, B.; Tsui, J. H.; Millik, S. C.; Shafranek, R. T.; Kim, D. H.; Nelson, A. Additive Manufacturing of Bovine Serum Albumin-Based Hydrogels and Bioplastics. *Biomacromolecules* **2020**, *21* (2), 484–492. https://doi.org/10.1021/acs.biomac.9b01236.

(30) Xue, D.; Zhang, J.; Wang, Y.; Mei, D. Digital Light Processing-Based 3D Printing of Cell-Seeding Hydrogel Scaffolds with Regionally Varied Stiffness. *ACS Biomater. Sci. Eng.* **2019**, *5* (9), 4825–4833. https://doi.org/10.1021/acsbiomaterials.9b00696.

(31) Wilts, E. M.; Pekkanen, A. M.; White, B. T.; Meenakshisundaram, V.; Aduba, D. C.; Williams, C. B.; Long, T. E. Vat Photopolymerization of Charged Monomers: 3D Printing with Supramolecular Interactions. *Polym. Chem.* **2019**, *10* (12), 1442–1451. https://doi.org/10.1039/c8py01792a.

(32) Fantino, E.; Roppolo, I.; Zhang, D.; Xiao, J.; Chiappone, A.; Castellino, M.; Guo, Q.; Pirri, C. F.; Yang, J. 3D Printing/Interfacial Polymerization Coupling for the Fabrication of Conductive Hydrogel. *Macromol. Mater. Eng.* **2018**, *303* (4), 1–8. https://doi.org/10.1002/mame.201700356.

(33) Palaganas, N. B.; Mangadlao, J. D.; De Leon, A. C. C.; Palaganas, J. O.; Pangilinan, K. D.; Lee, Y. J.; Advincula, R. C. 3D Printing of Photocurable Cellulose Nanocrystal Composite for Fabrication of Complex Architectures via Stereolithography. *ACS Appl. Mater. Interfaces* **2017**, *9* (39), 34314–34324. https://doi.org/10.1021/acsami.7b09223.

(34) Siqueira, G.; Kokkinis, D.; Libanori, R.; Hausmann, M. K.; Gladman, A. S.; Neels, A.; Tingaut, P.; Zimmermann, T.; Lewis, J. A.; Studart, A. R. Cellulose Nanocrystal Inks for 3D Printing of Textured Cellular Architectures. *Adv. Funct. Mater.* **2017**, *27* (12), 1604619. https://doi.org/10.1002/adfm.201604619.

(35) Ouyang, L.; Highley, C. B.; Rodell, C. B.; Sun, W.; Burdick, J. A. 3D Printing of Shear-Thinning Hyaluronic Acid Hydrogels with Secondary Cross-Linking. *ACS Biomater. Sci. Eng.* **2016**, *2* (10), 1743–1751. https://doi.org/10.1021/acsbiomaterials.6b00158.

(36) Yin, M. J.; Yao, M.; Gao, S.; Zhang, A. P.; Tam, H. Y.; Wai, P. K. A. Rapid 3D Patterning of Poly(Acrylic Acid) Ionic Hydrogel for Miniature PH Sensors. *Adv. Mater.* **2016**, *28* (7), 1394–1399. https://doi.org/10.1002/adma.201504021.

(37) Pawar, A. A.; Saada, G.; Cooperstein, I.; Larush, L.; Jackman, J. A.; Tabaei, S. R.; Cho, N.-J. J.; Magdassi, S. High-Performance 3D Printing of Hydrogels by Water-Dispersible Photoinitiator Nanoparticles. *Sci. Adv.* **2016**, *2* (4), 1–8. https://doi.org/10.1126/sciadv.1501381.

(38) Larush, L.; Kaner, I.; Fluksman, A.; Tamsut, A.; Pawar, A. A.; Lesnovski, P.; Benny, O.; Magdassi, S. 3D Printing of Responsive Hydrogels for Drug-Delivery Systems. *J. 3D Print. Med.* **2017**, *1* (4), 219–229. https://doi.org/10.2217/3dp-2017-0009.

(39) Shen, Y.; Tang, H.; Huang, X.; Hang, R.; Zhang, X.; Wang, Y.; Yao, X. DLP Printing Photocurable Chitosan to Build Bio-Constructs for Tissue Engineering. *Carbohydr. Polym.* **2020**, *235* (October 2019), 115970. https://doi.org/10.1016/j.carbpol.2020.115970.

(40) Yeh, Y.-C.; Highley, C. B.; Ouyang, L.; Burdick, J. A. 3D Printing of Photocurable Poly(Glycerol Sebacate) Elastomers. *Biofabrication* **2016**, *8* (4), 045004. https://doi.org/10.1088/1758-5090/8/4/045004.

(41) Heo, D. N.; Lee, S. J.; Timsina, R.; Qiu, X.; Castro, N. J.; Zhang, L. G. Development of 3D Printable Conductive Hydrogel with Crystallized PEDOT:PSS for Neural Tissue Engineering. *Mater. Sci. Eng. C* **2019**, *99* (September 2018), 582–590. https://doi.org/10.1016/j.msec.2019.02.008.

(42) Hiller, A.; Borchers, K.; Tovar, G. E. M.; Southan, A. Impact of Intermediate UV Curing and Yield Stress of 3D Printed Poly(Ethylene Glycol) Diacrylate Hydrogels on Interlayer Connectivity and Maximum Build Height. *Addit. Manuf.* **2017**, *18*, 136–144. https://doi.org/10.1016/j.addma.2017.10.008.

(43) Larrañaga, A.; Petisco, S.; Villanueva, R.; Iturri, J. J.; Moya, S.; Meaurio, E.; Sarasua, J. R. Physicochemical Properties of Plasma Polymerized Acrylic Acid, ε-Caprolactone and Lactic Acid Films. *Soc. Plast. Eng. - EUROTEC 2011 Conf. Proc.* **2011**, No. April 2016.

(44) Van Berkum, S.; Dee, J. T.; Philipse, A. P.; Erné, B. H. Frequency-Dependent Magnetic Susceptibility of Magnetite and Cobalt Ferrite Nanoparticles Embedded in PAA Hydrogel. *Int. J. Mol. Sci.* **2013**, *14* (5), 10162–10177. https://doi.org/10.3390/ijms140510162.

(45) Ollagnier, J. N.; Tassaing, T.; Harrisson, S.; Destarac, M. Application of Online Infrared Spectroscopy to Study the Kinetics of Precipitation Polymerization of Acrylic Acid in Supercritical Carbon Dioxide. *React. Chem. Eng.* **2016**, *1* (4), 372–378. https://doi.org/10.1039/c6re00022c.

(46) Liliang, O.; Rui, Y.; Yu, Z.; Wei, S. Effect of Bioink Properties on Printability and Cell Viability for 3D Bioplotting of Embryonic Stem Cells. *Biofabrication* **2016**, *8* (3), 35020.